JACS
JOURNAL OF THE AMERICAN CHEMICAL SOCIETY
Article
pubs.acs.org/JACS

Recognition of Imipenem and Meropenem by the RND-Transporter MexB Studied by Computer Simulations

Francesca Collu,[†] Attilio V. Vargiu,[‡] Jürg Dreier,[¶] Michele Cascella,*[,†] and Paolo Ruggerone*[,§]

[†]Departement für Chemie und Biochemie, Universität Bern, Freiestrasse 3, CH-3012 Bern, Switzerland
[‡]CNR-IOM, Unità SLACS, S.P. Monserrato-Sestu Km 0.700, I-09042 Monserrato (CA), Italy
[¶]Basilea Pharmaceutica International Ltd., Grenzacherstrasse 487, CH-4005 Basel, Switzerland
[§]Department of Physics, University of Cagliari, S.P. Monserrato-Sestu Km 0.700, I-09042 Monserrato (CA), Italy

Supporting Information

ABSTRACT: Basic understanding of the means by which multidrug efflux systems can efficiently recognize and transport drugs constitutes a fundamental step toward development of compounds able to tackle the continuous outbreak of new bacterial strains resistant to traditional antibiotics. We applied a series of computational techniques, from molecular docking to molecular dynamics simulations and free energy estimate methods, to determine the differences in the binding properties of imipenem and meropenem, two potent antibiotics of the carbapenem family, to MexB, the RND transporter of the major efflux system of *Pseudomonas aeruginosa*. We identified and characterized two affinity sites in the periplasmic domain of the transporter, sharing strong similarities with the distal and proximal binding pockets identified in AcrB, the homologue of MexB in *Escherichia coli*. According to our results, meropenem has a higher affinity to the distal binding pocket than imipenem while both compounds are weakly bound to the proximal pocket. This different behavior is mainly due to the hydration properties of the nonpharmacophore part of the two compounds, being that of imipenem less bulky and hydrophobic. Our data provide for the first time a rationale at molecular level for the experimental evidence indicating meropenem as a compound strongly affected by MexB contrary to imipenem, which is apparently poorly transported by the same pump.

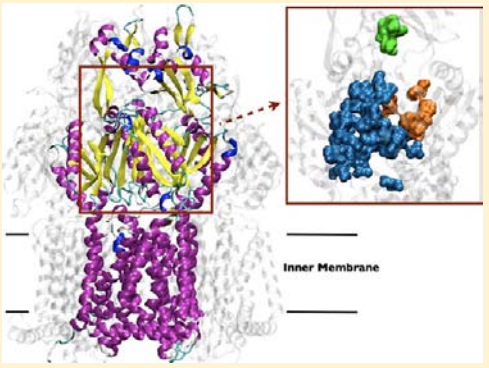

INTRODUCTION

The growing appearance of bacterial strains resistant to multiple, chemically unrelated antibiotics poses a great threat to public health. In particular, the dissemination of multidrug resistant (MDR) Gram-negative bacteria drastically impairs the efficacy of antibiotics of various families and limits their clinical uses.[1−6] Specifically, MDR *Pseudomonas aeruginosa* can generate life-threatening infections that are difficult to treat[7−10] and have been described in patients with cystic fibrosis, immunocompromised conditions and in isolated outbreaks in intensive care units.[11−15] Reports on critically ill patients in nonoutbreak settings have raised concerns because of the scarcity of novel agents to effectively treat MDR *P. aeruginosa* infections.[10,16−19]

Mechanisms associated with modifications of membrane permeation processes, such as decreasing the passive uptake (influx) or increasing the active efflux of antibiotics, are reported as key contributors to bacterial MDR.[20−28] Poly-specific efflux transporters, especially those belonging to resistance-nodulation division (RND) family,[21−24,27,29,30] confer a first-line resistance phenotype that can favor the acquisition and reinforcement of additional mechanisms of resistance, such as mutation of antibiotic targets (e.g., mutation in gyrase) or production of enzymes that degrade antibiotics (e.g., β-lactamases).[22,23,31]

The MexAB-OprM efflux complex is largely responsible for expulsion of several antimicrobial agents from *P. aeruginosa*.[19,22,23,28,31] This complex consists of a tripartite assembly[32] of MexB, an active transporter, OprM, a β-barrel shaped channel, and MexA, a fusion protein. MexB is partly embedded in the inner membrane and works as a drug/proton antiporter fueled by the transmembrane electrostatic gradient. OprM crosses the outer membrane and MexA stabilizes the connection between the other two components. MexB, the heart of the system, is a homotrimer consisting of a transmembrane domain with 12 membrane-spanning α-helices embedded in the inner membrane, and a large periplasmic domain. Recognition and binding of the substrates occur in this latter domain.

AcrB, the homologous protein of MexB in *Escherichia coli*, has been extensively characterized by X-ray crystallography both in the apo form and in complex with different ligands.[33−38] This wealth of data has allowed a proposal of a drug transport mechanism, in which each monomer neatly

Received: August 6, 2012
Published: November 12, 2012

   dx.doi.org/10.1021/ja307803m | J. Am. Chem. Soc. 2012, 134, 19146−19158

assumes in a succession of steps each of three conformations denoted as Loose (L), Tight (T), and Open (O), following the notation of Seeger et al.[35] The L, T, and O conformations[39] are associated with the access, binding, and extrusion of the substrate, respectively. This *functional rotation*,[34,35] driven by a transmembrane proton translocation, starts with the binding of substrates to an affinity site in the monomer with the L configuration, changed successively to T resulting in tight binding of the substrate, and finally converted to O with the release of the substrate toward the channel crossing the outer membrane. The O stage finally returns to L restarting the cyclic event.

With only one crystal structure of the apo protein published,[40] the structure of MexB is not so well characterized as that of AcrB. Nonetheless, several key structural features in MexB can be mapped on the structure of AcrB thanks to their close evolutionary proximity (69.8% identity in a sequence of 1046 amino acids). Of particular importance is the conservation of two crucial regions identified in AcrB as affinity sites of substrates. These are the Distal Binding Pocket (DP), a phenylalanine-rich pocket,[34,38] and the region called Proximal Binding Pocket (PP),[38,41] which is located close to the protein/periplasm interface. These correspondences suggest a similar binding and transport mechanism to take place in MexB and AcrB, stimulating the search for the general means by which a drug can be made resilient in the bacterial periplasm, hindering its capture by efflux systems. This aspect is crucial for the rational design of new antibiotics. Unfortunately, standard protocols, like high-throughput screening, have demonstrated their weaknesses in addressing the intrinsic complexity of MDR mechanisms.[42] An alternative route for the research of new antibiotics and of efflux inhibitors requires a microscopically well-founded knowledge of the dynamical interaction mechanisms between drugs and targets.[43−47]

In this last years, computer modeling has proved to be a valuable tool for investigating properties of RND-transporters at molecular level.[6,48−52] Following this route, we used different computational methods to investigate the impact of the interaction network, structural and dynamical features of MexB on the activity of imipenem and meropenem (Figure 2), both belonging to the class of carbapenems. Carbapenems, together with cephalosporins (i.e., cefepime), are commonly used to treat various infections by *P. aeruginosa*,[53,54] and imipenem and meropenem have been the most active broad-spectrum antimicrobial compounds documented by numerous large surveillance programs.[55] However, emergence of resistance has been reported.[10,56−58] Several studies, based on the evaluation of MICs, have pointed out the different influence of the MexAB-OprM system on the activity of the two antibiotics: meropenem is significantly affected, whereas imipenem is not.[59−62] Although it can be shown that efflux has a strong effect on MIC, it is very difficult to quantitatively determine the contribution of drug transport among all factors affecting the susceptibility of a cell to antibiotics.[63,64] Computer simulations are an important tool to bridge this gap and to complement and interpret experiments on kinetics.[65] The two carbapenems are very attractive candidates for a comparative study aimed at identifying the determinants of the carbapenem-efflux-pump interactions. In particular, the interaction of the substrates with MexB is crucial, as this unit is responsible for drug recognition, uptake, and transduction in the first steps of the extrusion process.

To our knowledge, this is the first computational study of antibiotic−MexB interactions. Extensive flexible blind docking calculations yielded possible affinity binding regions of meropenem and imipenem in MexB. These poses represented the starting configurations for all-atom molecular dynamics (MD) simulations. Albeit accurate, docking poses require a thorough validation via MD simulations. The experimental evidence of a multistep nature of the binding process, associated with the intrinsic polyspecificity of MexB, make MD simulations well suited to characterize the affinity of the ligands and to identify the key ligand−transporter interactions. Our results indicate that meropenem has a stronger preference for the DP than for the PP, while imipenem shows nearly the same low affinity for the two pockets. Analyses of our data point at the different hydrophobicity of the two carbapenems as the key factor for their different binding and transport properties in MexB.

MATERIALS AND METHODS

System Setup. We considered the crystallographic structure of MexB (PDB code: 2V50)[40] in the LTO asymmetric conformation as starting conformation for our study. The residues not resolved by X-ray diffraction were added to the protein using the MODELLER package.[66,67] Missing hydrogen atoms were added according to standard protonation states at pH 7.0. Residues Asp407, Asp408, Lys939 and Arg971 were protonated following ref 68.

The protein was placed in a 1-palmitoyl-2-oleoyl-sn-phosphatidylethanolamine (POPE) phospholipid bilayer (677 molecules) and solvated with 81 921 water molecules. Thirty-seven Na^+ counterions were added to neutralize the system, which resulted in a total of 378.552 atoms. The structure of the protein was relaxed in the presence of harmonic restraints (k = 1 kcal·mol^{-1}·Å^{-2}) on C_α atoms, as to remove potential steric clashes. The presence of soft restraints on C_α's ensured that the global asymmetry of the complex skeleton was not compromised, while the presence of waters and the lipid bilayer guaranteed that side-chain reorientations occurred in an environment as close as possible to the real one.

The potential function for our system was built using the PARM99SB AMBER force field[69,70] for the MexB, the TIP3P model for water,[71] and the Aqvist parameters[72] for the ions. For POPE we used the parameters developed in recent works.[48]

Structural optimization was performed with the conjugated gradient scheme implemented in NAMD.[73] After about 10 000 steps, energy and structural convergence was reached, and the final C_α and all-atoms (not including hydrogens) RMSDs from the X-ray structure were 0.3 and 1.2 Å, respectively. The structure of MexB, extracted from this structural relaxation, was used for subsequent flexible molecular docking.

We developed the force-field parameters for imipenem and meropenem (Figure 2) following the AMBER protocol.[69] The GAFF force-field[74] was used to describe bonded and van-der-Waals interactions. Point charges for these molecule were derived using standard RESP procedure,[75] assuming both compounds in their neutral forms (Figure 2).

To obtain the starting ligand structures for the docking, 10 ns-long MD simulations (see Molecular Dynamics Simulation section) of the two carbapenems in a box of water were used to identify significant representatives of the two compounds via a cluster analysis of the trajectories. Meropenem conformations were grouped in two main clusters with populations of 50.5% and 38.2% of the total number of sampled structures. Imipenem configurations were mapped instead onto three distinct clustered geometries with 40.1%, 27.6%, and 3.9% relative populations. For both molecules, the remaining poses were partitioned over several clusters of single or very few poses, and thus, they were not considered in the present analysis. Representative structures of the largest clusters (Figure 2) were used as starting conformations for flexible blind docking[76,77] on MexB.

Molecular Docking. The structures of the complexes of MexB with imipenem and meropenem were obtained by flexible molecular docking using the ATTRACT package.[76,77] The program accounts for global flexibility of the protein and the two carbapenems by considering deformations along the normal modes[78] as collective degrees of freedom in the docking runs,[77] and performs an energy minimization search in the conformational space defined by the six rototranslational-degrees of freedom of the ligand and the five low-frequency normal modes for both the protein and the ligand. To speed up the calculations, ATTRACT adopts a reduced pseudo-atom representation to represent both docking partners. In ATTRACT the docking of a ligand can be biased toward a certain region by applying an harmonic force between the center of mass of the ligand and a pulling center located in the region of interest. In our case, since no binding pocket has been identified on MexB yet, we set the pulling center at the center of mass of the periplasmic domain. Docking runs were performed on a truncated model of MexB, including only the periplasmic domain, as this is the region responsible for selectivity, involved in recognition and binding of substrates. One thousand initial starting positions of the center of mass of the ligand were considered, localized on points of a 5 Å-meshed grid embedding the protein. For each of these positions, 300 different ligand orientations were generated, for a total of 300 000 starting configurations.

Molecular Dynamics Simulation. The best poses identified by ATTRACT for meropenem and imipenem in DP and PP were chosen as starting configurations for MD simulations performed with the NAMD package.[73] The force field parameters used in the simulations were described in the System Setup section. We solvated each truncated complex with 45 000 water molecules, obtaining four systems (one for each drug in each pocket) of 160 000 atoms in a orthorhombic box. At first, the complexes were relaxed by 5000 steps of minimization procedure (500 steps of steepest descent and 4500 steps of conjugate gradient minimization). After structural optimization, the systems were gradually heated in the NVT ensemble from 0 to 310 K over 100 ps using a Langevin thermostat[73] to control the temperature. We then performed MD simulations of 5 ns in the NpT ensemble to equilibrate the volume of the box, targeting the pressure to 1 atm via a Berendsen barostat.[79] Successively, MD simulations lasting 50 ns in the NpT ensemble at 310 K and 1 atm were performed. We ran a total of 4 simulations, one for each configuration of the substrate. Constant temperature and pressure conditions were maintained by application of Langevin temperature and pressure controls as implemented in NAMD.[73] Periodic boundaries were applied, electrostatic interactions were computed using soft particle mesh Ewald scheme[80] with a real-space cutoff of 12 Å. Bonds involving hydrogen atoms were fixed using the SHAKE algorithm.[81] We adopted a time step of 2 fs for the integration of the equations of motion. The equilibrated box had dimensions of 131.0 × 129.4 × 113.3 Å^3.

System setup and data analysis were done with xleap of the Amber11 package[82] and the VMD program.[79]

Analysis of Ligand−Solvent and Ligand−Protein Interactions. The survival probability for water molecules bound to the compounds was calculated as reported by Sterpone et al.[83] considering the 50 ns-long MD trajectories. To distinguish among three different time regimes (fast, medium, slow residence times), we used the following function:

$$F(t) = n_{fast}\exp\left[\left(-\frac{t}{\tau_{fast}}\right)^{c}\right] + n_{medium}\exp\left(-\frac{t}{\tau_{medium}}\right) + n_{slow}\exp\left(-\frac{t}{\tau_{slow}}\right) \quad (1)$$

to fit the survival probability and extract the different temporal scales and the associated number of water molecules. In eq 1, the first term corresponds to fast regime (less than 50 ps), the second to medium regime (around 500 ps) and the last term to slow regime (greater than 1000 ps). The variables τ_{fast}, τ_{medium}, and τ_{slow} are the different relaxation times and n_{fast}, n_{medium}, n_{slow} are the average number of water molecules in the three regimes.

The hydrogen bonds contacts between the substrate and the transporter were defined using cutoff values of 3.0 Å for acceptor−donor distance and 130° for acceptor−donor angle. Hydrophobic contacts were counted when nonpolar atoms were separated by at most 4.0 Å.

Binding Free Energy Calculations. Binding free energies for both ligands were estimated by combining the thermodynamic cycle of Figure 3 and MD simulations. Following this approach,[84] the binding energy is estimated by splitting the calculation in the evaluation of the binding energy *in vacuo* and the effect of solvation on each state of the system: the complex, both the ligand and the protein separately. The equation associated with the thermodynamic cycle is the following:

$$\Delta G_{bind} = \Delta G_{solv}^{Complex} - \Delta G_{solv}^{Ligand} - \Delta G_{solv}^{Receptor} + \Delta G_{gas} \quad (2)$$

where $\Delta G_{solv}^{Receptor}$, ΔG_{solv}^{Ligand}, and $\Delta G_{solv}^{Complex}$ are the solvation free energies of the protein, the ligand, and the complex, respectively, while $\Delta G_{gas} = \Delta E_{gas} - T\Delta S_{gas}$ is the binding free energy for the complex *in vacuo*. The two terms contributing to ΔG_{gas}, that is, ΔE_{gas} and ΔS_{gas}, represent the energy of binding and the binding entropy *in vacuo*.

The MM/PBSA protocol[85−87] implemented in the Amber11 package[82] was used to calculate the solvation energies by solving the Linearized Poisson−Boltzmann equation using dielectric constants of ε = 1 and 80 to reproduce the *in vacuo* and *in solvent* conditions, respectively.[88] The binding energy ΔE_{gas} was estimated using the same force field used also for the simulation. We evaluated ΔS_{gas} within the framework of the Quasi-harmonic approximation, whose details and limits are deeply discussed in the literature.[89−94]

For MM/PBSA calculations, we extracted one structure every 500 ps from three 50 ns-long MD trajectories in order to get uncorrelated snapshots for the calculation. We used 100 independent structures to obtain all solvation-related quantities and the binding energy in eq 2. The ΔS_{gas} were calculated during the whole 50 ns of the production MD run using all saved frames (25 000). As entropy is a time-dependent parameter, 50 ns were chosen to obtain as much convergence as possible.[84]

RESULTS

We focused our analysis on the binding properties of imipenem and meropenem to the PP and DP of the T monomer (Figure 1). In AcrB, both PP and DP are open and ready to

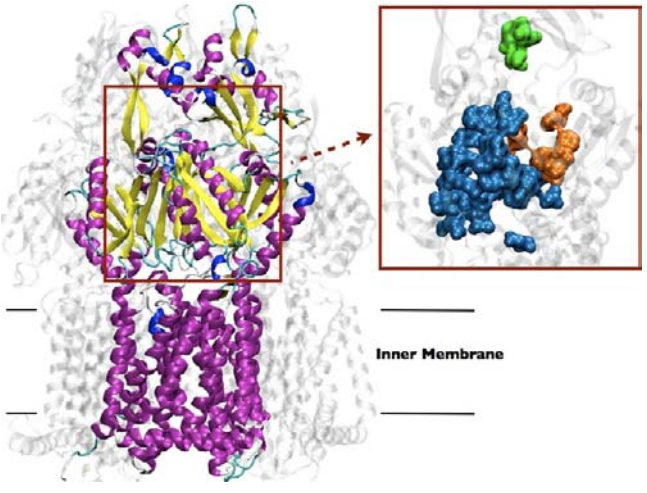

Figure 1. Structure of MexB. T monomer is colored according to its secondary structure elements, the O, L monomers are in gray transparent representation. The localization of the inner membrane is depicted by horizontal black lines. Inset: the residues identifying the PP, DP and *Gate* of the T monomer are represented in surface, and colored in blue, orange, and green, respectively. For a detailed list of the residues defining these regions, see Table 1.

Table 1. Residues Defining Regions of MexB Discussed in the Text

region	residues
Proximal Binding Pocket (PP)	Gln46, Arg76, Tyr77, Ser79, Glu81, Thr89, Thr91, Lys134, Asn135, Lys292, Asp566, Val571, Phe573, Gln575, Ser576, Gln577, Gly614, Phe617, Gly619, Arg620, Gly621, Ser624, Met662, Phe664, Phe666, Pro668, Pro669, Leu672, Glu673, Leu674, Gly675, Asn676, Ala677, Phe680, Asp681, Arg716, Asn718, Glu825, Thr859, Glu864, Glu865
Distal Binding Pocket (DP)	Phe136, Val139, Gln176, Phe178, Ile277, Phe281, Ala290, Tyr327, Phe573, Phe610, Phe615, Phe617, Phe628
Channel	Ser48, Tyr49, Pro50, Gly86, Ser87, Met88, Ile127, Arg128, Val177, Phe178, Gly179, Ser180, Gln181, Gln273, Asp274, Tyr275, Ser276, Trp754, Val767, Lys768, Arg769, Val770, Tyr771, Tyr772
Gate	Arg124, Gln125, Tyr757

accommodate a substrate in the T and L monomers, respectively,[34,38,41] with the PP featuring a wide entrance cleft on the periplasmic side. Unlike AcrB, in the crystal structure of MexB both pockets can be identified only in the T monomer, which presents the widest opening of the external cleft.[40] The particularly narrow configuration of the PP in the L monomer makes binding to this site very unlikely. Thus, the PP represents a probable affinity site in the T monomer not least because it is located at the periplasmic side of the subunit and it might be involved in the early steps of the recognition.

Although there is no direct evidence that the DP is an affinity site in MexB, this part of the protein is identical, in both its sequence and structure, to the DP in homologous AcrB. It is mainly lined by hydrophobic residues (Phe) and has one opening toward the PP and a second one toward the channel leading to the *Gate*. The latter is a crucial passageway during the translocation of the drugs from the DP toward the OprM channel. The DP−*Gate* connection region (hereafter named *Channel*) is delimited by essentially hydrophilic residues as in the case of AcrB. The residues defining the PP, DP, *Channel*, and *Gate* are listed in Table 1.

Docking of Imipenem and Meropenem on MexB. Representative structures of the top clusters extracted from simulations of imipenem and meropenem in a box of water (Figure 2) were used as starting conformations for flexible blind docking[76] on MexB, following the procedure described in Materials and Methods. The docking center was located in the center of mass of the periplasmic domain, which is the region involved in recognition and binding of substrates.

Nearly all the poses for both compounds were located in the T monomer, to which substrates supposedly bind the tightest. Table S1 (Supporting Information) contains a list of the residues within 3 Å from the two carbapenems in the relevant poses extracted from docking. It is worth pointing out that we also obtained some poses located in the L monomer but only by placing the docking center in the region around the DP of that monomer, thus, by biasing the pose search in that region. Moreover, these poses were characterized by poorer scoring functions and lower cluster populations than the poses obtained in the T monomer assuming the center of mass of the periplasmic domain as the docking center.

The PP, close to the protein/periplasm interface, should be visited before the DP along the path of most substrates from the periplasmic space. In our docking calculations, a small percentage of poses were found here (0.3−0.4% of the entire population for both carbapenems) with scoring energies of ≈−11.7 and ≈−8.3 kcal/mol for meropenem and imipenem, respectively. Figure 4 (panels a and b) shows the docking geometries for meropenem and imipenem in these poses. The binding orientations of the two carbapenems shared some similarities, with the β-lactam ring displaced toward the protein and the tail of the molecule facing the bulk solvent. However,

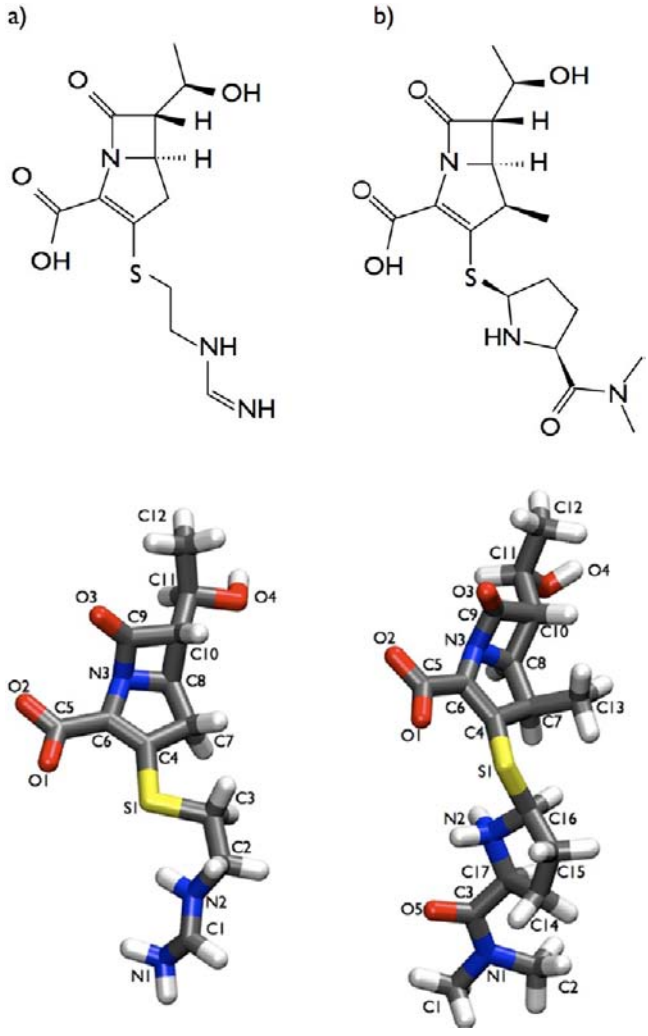

Figure 2. Chemical structures (upper row) and three-dimensional representation with atom labels (lower row) of (a) imipenem and (b) meropenem. The three-dimensional representation brings the protonation states for the titrable groups used in the simulations.

meropenem penetrated more deeply into the protein than imipenem. Hydrophobic interactions were present between the atoms C14 and C15 of the meropenem tail ring and Phe617, a residue belonging to the G-rich loop defining the border between the PP and the DP.[38] The β-lactam ring of imipenem made hydrophobic interactions with Leu674 and Phe617, while the tail remained exposed to the solvent.

The next binding region of the protein probably found by ligands during the translocation through MexB is the DP. Top poses of the two carbapenems in the DP are shown in Figure 4 (panels c and d). Significant differences were observed in the interactions of the two compounds with MexB. First, only very

dx.doi.org/10.1021/ja307803m | J. Am. Chem. Soc. 2012, 134, 19146−19158

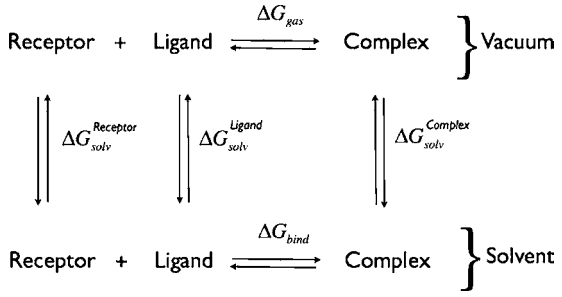

Figure 3. Thermodynamic cycle used for the computation of the free energy of binding. The free energy is decomposed in contributions coming from the solvation energy of the reactant and products, and from the binding free energy *in vacuo*.

few poses of imipenem were found in this pocket (covering totally ≈1.5% of the overall computed structures) while meropenem sat in the DP in ≈13% of the docking poses (1 order of magnitude greater). Second, the scoring energy of 9.2% of meropenem poses in the DP was ≈−17.0 kcal/mol, whereas for imipenem, we found only 2 poses over 30 000 (i.e., 0.007% of the poses) with a comparable scoring function. The remaining poses of imipenem had scoring energies between ≈−13.0 and ≈−16.0 kcal/mol. Third, the analysis of the configurations belonging to the top clusters highlighted a striking difference between the two compounds. Indeed, meropenem and imipenem had opposite orientation (cf. lower row in Figure 4). Meropenem was stabilized by hydrophobic interaction between its methyl group in C13 and Phe628, while imipenem established hydrophobic interactions between the methyl group in C12 of its β-lactam ring and Phe178 and between its S1 atom and Phe136.

The third crucial region found by ligands during the translocation process is the *Channel* from the DP to the *Gate*. Our docking runs yielded a good percentage of poses in this region (30.2−34.3% of the entire population for both carbapenems), with a scoring function of ≈−11.8 kcal/mol (meropenem) and ≈−17.7 kcal/mol (imipenem). Figure S1 (Supporting Information) shows the top poses of meropenem and imipenem in the *Channel*. The orientations of the two carbapenems shared some similarities, like the β-lactam ring displaced toward the *Gate* and the tail facing the DP. The position of meropenem was stabilized by the hydroxyl group of the β-lactam ring and the atom O5 of the tail, which H-bonded to Arg128 and Arg620, respectively. A single H-bond was formed between the carboxylic group of imipenem and the side chain of Arg128, and the other interactions of imipenem were with residues Ser48, Gln176, and Phe168 hydrophobic contacts.

A fourth set of docking poses was found in the large central pore of the extramembrane headpiece of the MexB trimer. Although originally proposed as part of a possible substrate translocation pathway,[95−99] the direct involvement of this large cavity in the extrusion process has been successively called into question.[68,100,101] Therefore, we excluded these poses from our refined analysis via MD simulations. Because our efforts focused on the early events in the translocation process, we did not analyze the poses located in the *Channel* either. This region should be touched by the ligands after the DP along the path toward the OprM docking domain.

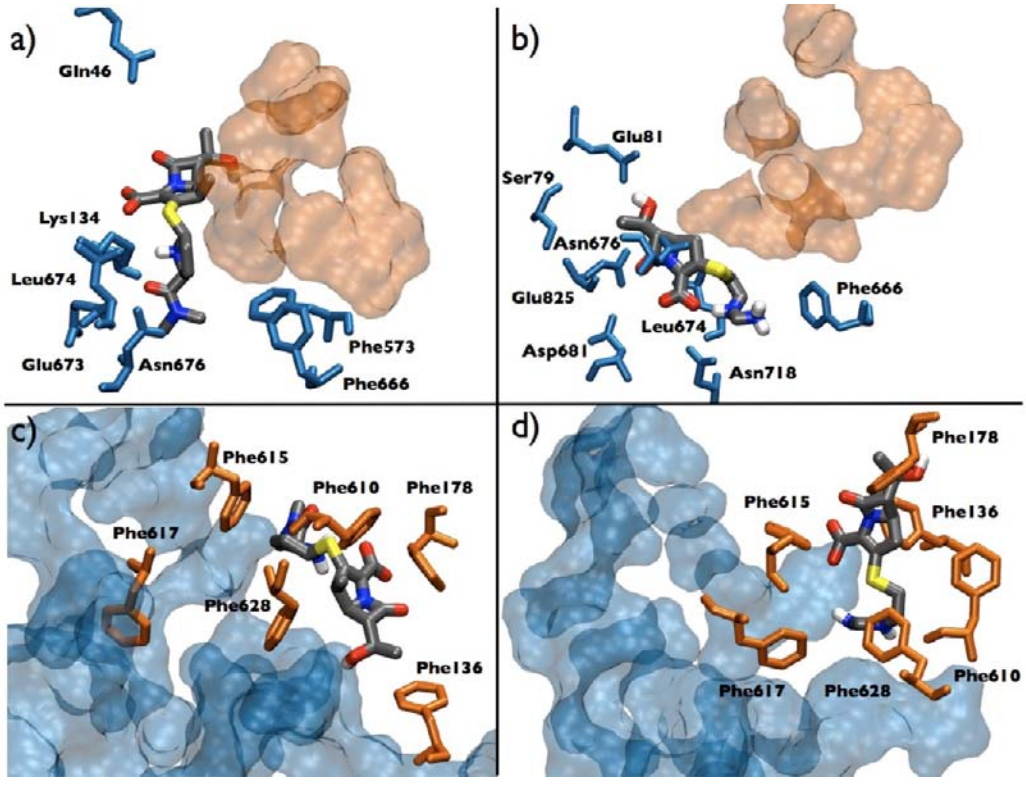

Figure 4. Selected poses of meropenem and imipenem in the PP and DP. (a and b) Binding configurations of meropenem (a) and imipenem (b) in the PP. Residues of the PP within 3 Å from the carbapenem molecules are represented in blue-colored licorice. (c and d) Binding configurations of meropenem (c) and imipenem (d) in the DP. Residues of the DP are drawn in orange-colored licorice. In all panels, the pocket not involved in the binding is represented in surface. For the sake of clarity, panels a and c are slightly rotated with respect to panels b and d, respectively.

dx.doi.org/10.1021/ja307803m | J. Am. Chem. Soc. 2012, 134, 19146−19158

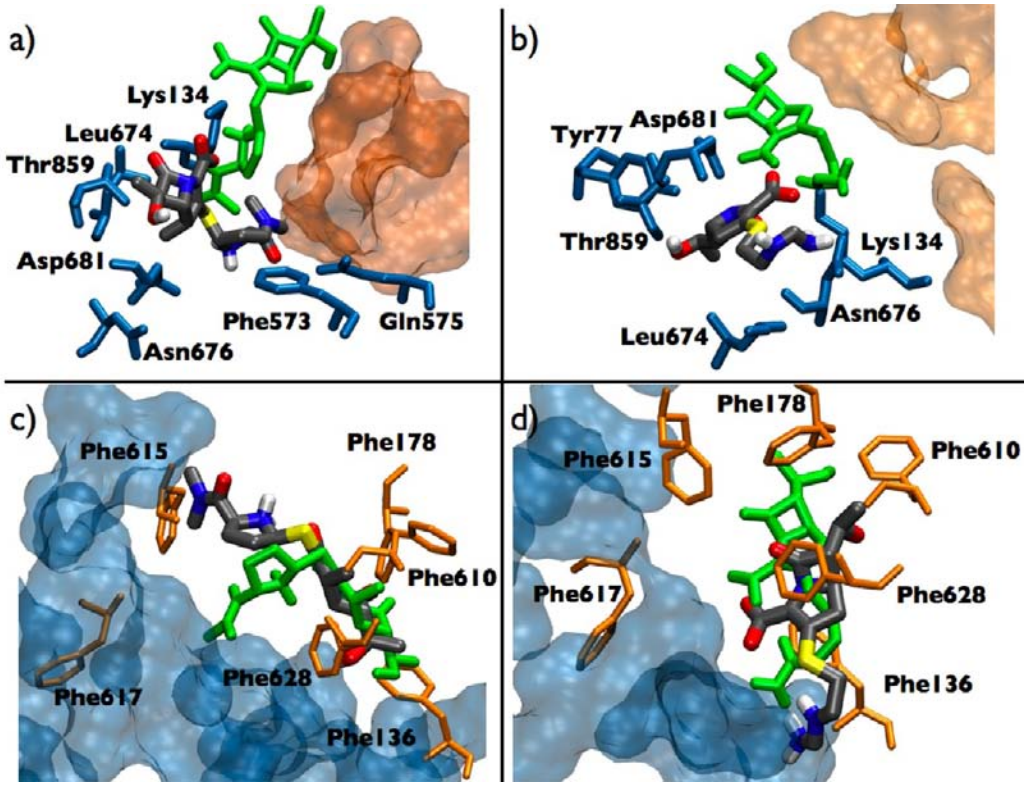

Figure 5. Initial and final configurations of meropenem and imipenem extracted from 50 ns-long MD simulations. In all panels, the starting configuration of the carbapenem is represented in green licorice, the final one in atom-code colored licorice. (a and b) Binding configurations of meropenem (a) and imipenem (b) in the PP. Residues of PP within 3 Å from the carbapenem molecules are represented in blue-colored licorice. (c and d) Binding configurations of meropenem (c) and imipenem (d) in the DP. Residues of the DP are drawn in orange-colored licorice. In all panels, the pocket not involved in the binding is represented in surface. For the sake of clarity, panels a and c are slightly rotated with respect to panels b and d, respectively.

MD Simulations. The docking results provided some evidence of significant differences in the molecular recognition of the two carbapenems in the first two affinity regions (PP and DP, see remarks at the beginning of the Results section). In particular, while in the PP both antibiotics interacted in the same fashion with MexB, meropenem had a stronger affinity to the DP than imipenem. However, the results of docking needed to be validated by more accurate methods, such as MD simulations, for at least two reasons: (a) the interaction of substrates with MexB is a multistep and dynamics-assisted binding process, as evidenced by experimental studies;[34,38,41] (b) the correlation between quality of the transport and substrate affinity is not straightforward,[51] which demonstrates how unpredictable the binding process is. Thus, starting from the docking poses of Figure 4, we performed 50 ns-long MD simulations to quantitatively assess stability and affinity of the two antibiotics in both PP and DP. Note that our attention focused on these two regions because we were interested in the first key steps of the binding process, aiming at identifying at this stage possible molecular determinants of the different interactions of the compounds with the transporter. To assess the structural convergence of the simulations, we checked that the RMSDs of the entire protein and of the single monomers reached stability after few nanoseconds (see Figure S2).

Initial and final configurations of the compounds in the PP and DP are shown in Figure 5. The two carbapenems behaved differently in the PP with respect to their initial position. The final conformations of the MD runs were characterized by a substantial difference (Figure 5): meropenem was oriented toward the entrance of the DP maintaining during the simulation a distance of ∼11 Å from the center of mass of the DP (see Figure S3) while imipenem had its head pointing toward the periplasmic region, outside the transporter, at ∼16 Å from the center of mass of the DP (initial distance: ∼13 Å, see Figure S3). Essentially, meropenem rotated during MD and pointed its tail toward the DP entrance. Imipenem changed its position by moving away from the starting location and approaching the protein-periplasm boundary.

In the DP, meropenem maintained essentially the same position identified by docking, close to the entrance of the *Channel* leading to the OprM docking domain, and aligned its axis with the direction of the extrusion path (Figure 5c). This tendency of meropenem was confirmed by the evaluation of the distances of the center of mass of the compound from its original position (Figures S4) and from the center of mass of the *Gate* (Figure S5). The slight increase of the distance with respect to the *Gate* was due to the rotation of the compound.

On the other hand, the position of imipenem found by docking in the DP resulted only marginally stable during equilibration, as the compound rapidly drifted toward the bottom region of the DP, away from the entrance of the *Channel* (Figure 5d). The overall shift of the center of mass of the molecule from its original position was ∼2.5 Å (see Figure S4) while the distance from the center of mass of the *Gate* increased from ∼26 to ∼30 Å (see Figure S5).

The dynamical response of the two compounds within PP and DP was monitored by computing their Root Mean Square Fluctuations (RMSFs), which is a measure of the local flexibility

dx.doi.org/10.1021/ja307803m | J. Am. Chem. Soc. 2012, 134, 19146−19158

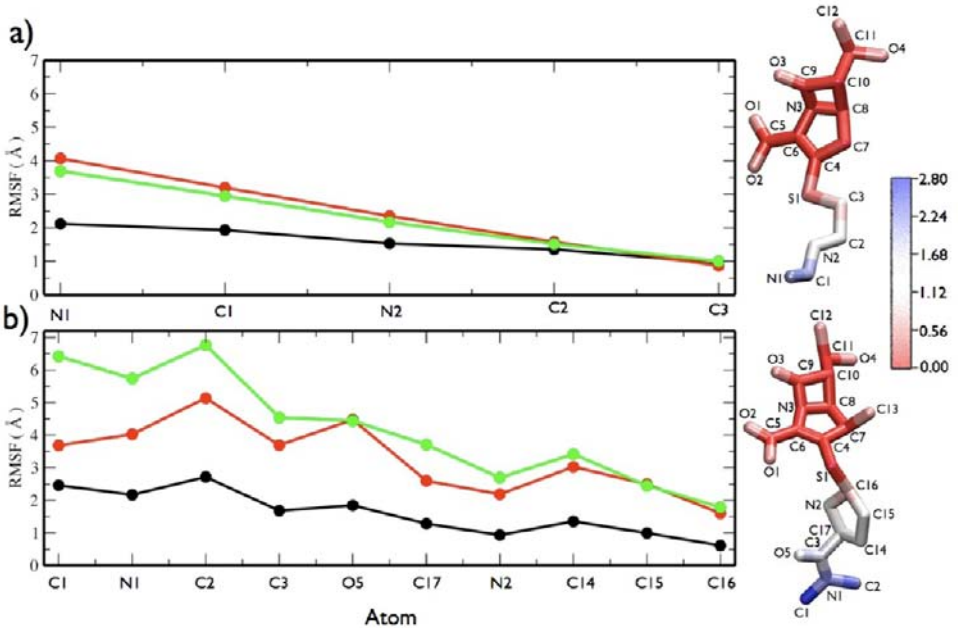

Figure 6. RMSF extracted from MD simulations (left panels) and visualization of the compounds according to their RMSF (right panels): (a) imipenem and (b) meropenem. In the left panels, only atoms having an RMSF larger than 1 Å are considered. Black curves refer to the compounds in the DP, green in the PP, and red in water box. The alignment was done on the bulky part of the compounds. The reference structures for each region are the average structures extracted from the MD simulations of the compounds in the region. The labeling of the atoms corresponds to Figure 2. In the right panels, atoms of the compounds are colored according to RMSF evaluated in the DP.

Table 2. Free Energies of Binding (ΔG) and Their Dissections in Enthalpic and Entropic Contributions for Imipenem and Meropenem in PP and DP[a]

	Imipenem			Meropenem		
position	ΔH	$T\Delta S$	ΔG	ΔH	$T\Delta S$	ΔG
DP	−15.4	−15.8	0.4 ± 3.8	−22.6	−14.5	−8.1 ± 4.5
PP	−12.7	−13.3	0.6 ± 7.0	−10.6	−13.0	2.4 ± 4.8

[a]All the values are in kcal/mol.

of the compounds, and by comparing them to the respective values in the solvent. In particular, we performed structural alignment on the rigid, bulky part of the compounds (the pharmacophore group) in order to compare the flexibility of the tail in the different environments. The results are reported in Figure 6. In the DP, the fluctuations of the two compounds were similar in magnitude while differences characterized the behavior in PP and in water. In these regions, the fluctuations with respect to the average structure were larger for meropenem than for imipenem. Additionally, the behavior of imipenem in PP and in water was essentially the same. This was confirmed also by the evaluation of the RMSF but referred to the average structure of the compounds in water (data not shown).

Binding Free Energies. The affinity of the two compounds for MexB in both the PP and DP regions were evaluated by estimating their binding free energies. The results are collected in Table 2. Note that the standard deviations increased significantly when the compounds were in the PP, which is consistent with the larger fluctuations of the two carbapenems in that region of the transporter. It clearly appeared that meropenem had a remarkable affinity for the DP but not for the PP. Here the calculated free energy of binding was positive, and the change in the sign of ΔG is essentially due to a strong decrease in the enthalpic contribution by going from the DP to the PP. On the other hand, imipenem did not seem to have a preferred affinity site, as the calculated free energies of binding were small, positive, and nearly the same at both DP and PP.

Analysis of Interactions of Imipenem and Meropenem with MexB. During the equilibrium trajectories considered in the present analysis, both ligands formed transient contacts with different amino acids of MexB. Those contacts observed for more than 2.5% of the total simulation time were considered as relevant for binding and are discussed here. This threshold was sufficient to eliminate several contacts that represented random noise in our systems.

Panels a and b of Figure 7 report the statistical distributions of the contacts of the residues defining PP with meropenem and imipenem, respectively. In this region, the two compounds behaved differently. In particular, meropenem made one statistically relevant contact with Lys134 (via its carboxylic group), while contacts with other regions of the PP were statistically less frequent. This H-bond showed also good resiliency, with average lifetime of ≈7 ns. Interestingly, Lys134 residue is located at the boundary between the PP and the DP. For imipenem, the contact distribution in the PP provided evidence of the regions explored by the compound (Figure 7). Initially, imipenem formed a significant H-bond between its hydroxyl group and the side-chain of Glu81 (36% of statistical probability). Successively, imipenem interacted also with Lys134 via an H-bond and then moved to a region of the PP close to the outer boundary of the protein and far away from

dx.doi.org/10.1021/ja307803m | J. Am. Chem. Soc. 2012, 134, 19146−19158

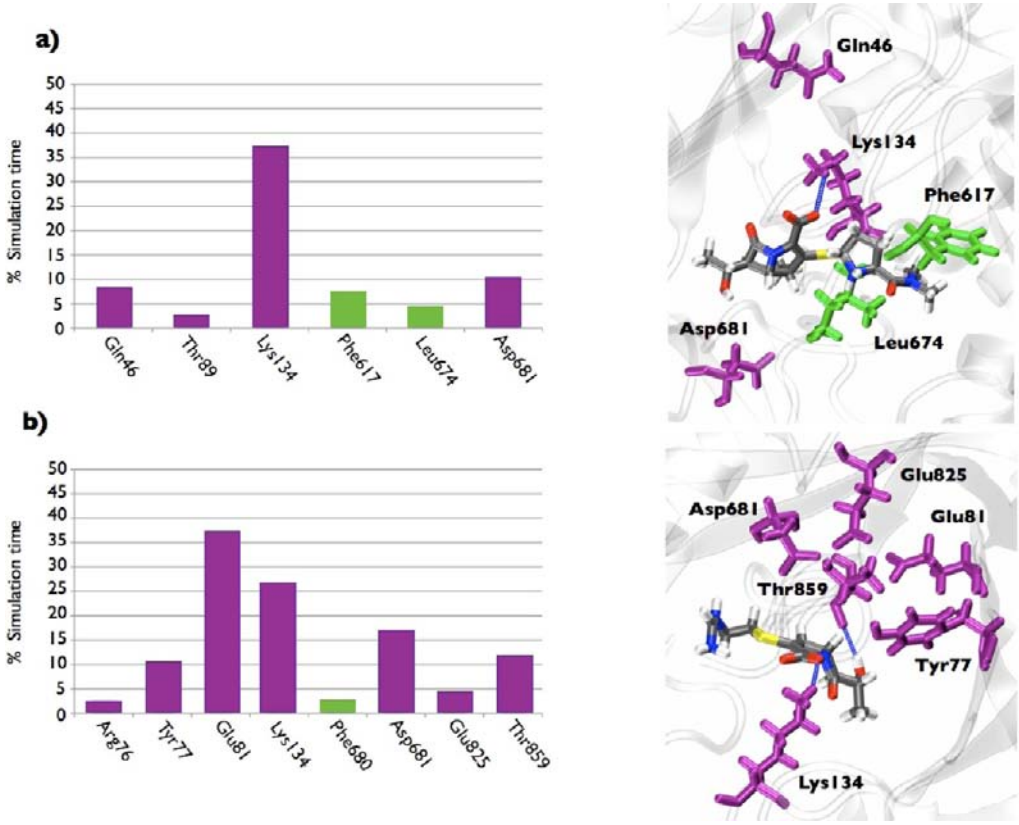

Figure 7. Statistical distribution (% of the total simulation time) of the direct contacts between residues and ligands when these latter are in the PP (left column) and positions of the residues appearing in the histograms (right column): (a) meropenem, (b) imipenem. For the sake of clarity, the panels of the right column have different orientations. Only the contacts observed for more than 2.5% of the simulation time are reported. Histograms for residues forming H-bond contacts with the substrate are colored in magenta, those associated to residues forming hydrophobic contacts are colored in green. The statistically most relevant configurations for the two compound are represented in the corresponding pictures to the right. The compounds in the configurations assumed at the end of the simulations are represented in licorice and colored by atom-code. Residues indicated in the graphs are represented in licorice and colored with the same code as that used the histograms. Blue springs identify H-bond. The data are extracted from standard MD simulations lasting 50 ns for each configuration.

the entrance to the DP. Imipenem formed additional, less stable, hydrophilic contacts with the PP. Specifically, it established H-bonds between its imino group and the side chain of Asp681 and between its hydroxyl moiety and the side chains of Thr859 and Tyr77. Hydrophobic contacts were characterized by a low statistical abundance, the only relevant contact being the one between the imino group of imipenem and the aromatic side chain of Phe680 (~3%). Interestingly, the interaction of imipenem with Leu 674 was present in the docking pose but did not occur with statistical relevance during MD simulations. On the contrary, interaction of meropenem with Leu 674 was established during the trajectory in the PP (~5%, Figure 7a). Leu674 is conserved in AcrB where it is located at the juncture between possible entrance channel at the interface between the DP and PP. A recent work of Nakashima et al.[38] on AcrB pointed out the effect of the L674W mutation on the resistance to doxorubicin and erythromycin. The mutant AcrB transported the two compounds at drastically lower rates. In MexB, the presence of an interaction between the carbapenems under investigation and Leu674 might be an indication of an involvement of Leu674 in uptake and/or transport of compounds belonging to an extended set of families, calling for additional experiments.

The binding geometries of meropenem and imipenem were remarkably different in the DP. Overall, meropenem made statistically more significant contacts than imipenem did. The distributions of the contacts in the DP are shown in Figure 8. Gln176, Phe178, and Leu672 interacted with both compounds although with different statistical frequencies. Meropenem preferentially made a H-bond to the carboxylic moiety of Glu673 as well as two other stable contacts with Phe178 and Gln176. The contact with Phe178 had hydrophobic character (T-shaped stacking between the phenyl group and the condensed dehydro-pyrrole ring of the drug), the one with Gln176 was achieved by H-bond donation of the side chain amide group either to the hydroxyl oxygen or to the lactam carbonyl oxygen atoms of meropenem. All durable contacts between meropenem and the protein involved chemical groups of the drug located in proximity of the β-lactam moiety while the contacts stabilizing meropenem and involving other parts of the compounds were much less frequent.

Imipenem made two contacts with an occurrence of roughly 20% of the simulation time: with Phe136, in a T-shape configuration similar to that seen for meropenem, and with Leu672, through H-bond formation between the amino acid carbonyl backbone and the imine nitrogen of imipenem. The only two other contacts, which were statistically significant, were H-bonds between the hydroxyl of the drug and the side chains of Gln176 and Lys134. Importantly, Lys134, which sits at the edge between the PP and the DP, made contact with imipenem in both pockets. This finding corroborated the evidence that imipenem highly preferred to form contacts with

dx.doi.org/10.1021/ja307803m | J. Am. Chem. Soc. 2012, 134, 19146−19158

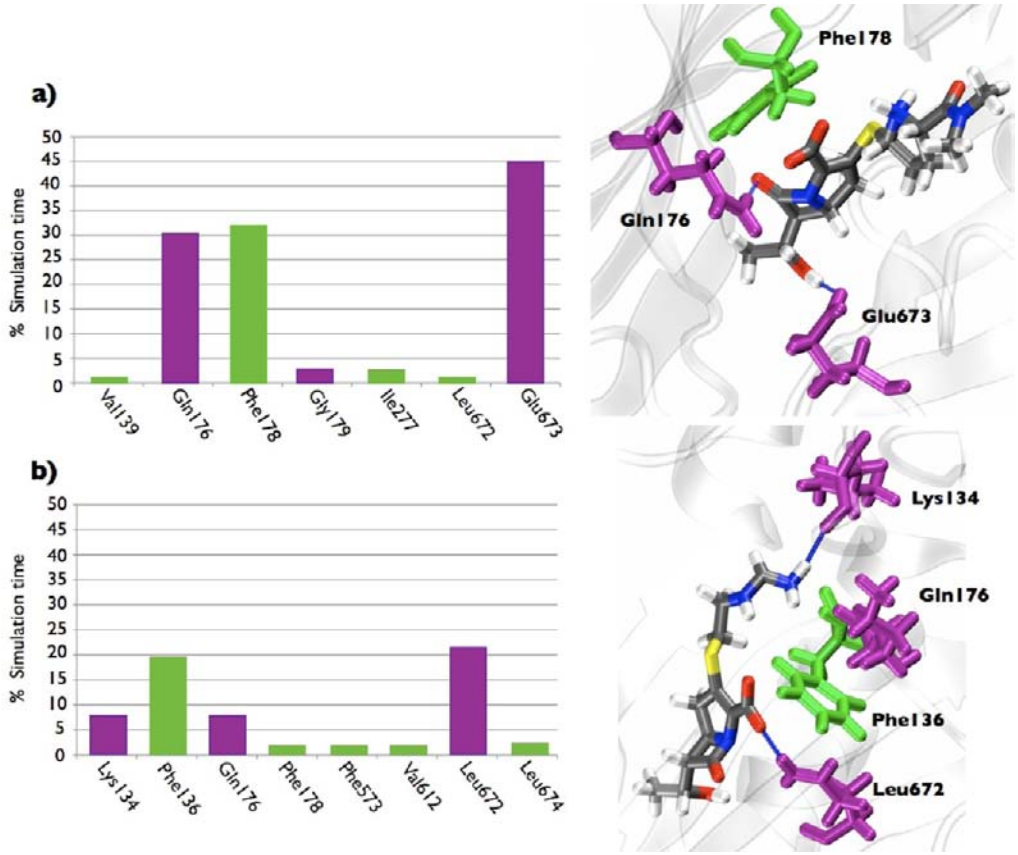

Figure 8. Statistical distribution (% of the total simulation time) of the direct contacts between MexB residues and ligands when these latter are in the DP (left) and positions of the residues appearing in the histograms (right): (a) meropenem, (b) imipenem. For details see caption of Figure 7.

Table 3. Analysis of Solvation Properties of Compounds in DP and PP[a]

	Imipenem				Meropenem			
	average number	fast (%)	medium (%)	slow (%)	average number	fast (%)	medium (%)	slow (%)
DP	11	0	62.1	37.9	18	83.3	16.7	0
PP	24	95.8	4.2	0	27	92.6	7.4	0
Water	38	100	0	0	45	100	0	0

[a]The average numbers of water surrounding imipenem and meropenem are collected in the second and sixth columns, respectively. The numbers of fast, medium, and slow waters are expressed in percentage of the average numbers. The corresponding values for the two compounds inserted in a bulk water box extracted from a 10 ns-long standard MD simulation are reported.

residues lining the entrance of the DP (e.g., Lys134, Phe136, Gln176) than meropenem did. These contacts involving imipenem occurred far away from the entrance to the *Channel* leading to the central funnel of the OprM docking domain.

Finally, it has to be pointed out that most of the stable protein/drug contacts in the PP were hydrophilic, whereas most contacts stabilizing the compounds in the DP were of hydrophobic nature. This was more evident for meropenem than for imipenem.

Interaction with Solvent. According to the results collected in Table 3, water molecules in contact with imipenem had distinctively longer interaction lifetimes than water molecules in contact with meropenem. This situation was observed in both PP and DP. Also water molecules of the *medium* class had longer exchange times with imipenem than they had with meropenem. For example, the medium waters in the PP had average residence times in the proximity of imipenem and meropenem of 824 and 584 ps, respectively.

The slow waters interacting with imipenem inside the DP formed H-bonds with the atoms N1, N2, O4, and with the carboxylate group (see Figure 9). These waters were within 3 Å from the residues Lys134, Val139, Pro326, Tyr327, Thr329, Leu672, and Leu674.

DISCUSSION

The results obtained in our study indicate a possible rationale for the different influence of MexB on the activity of imipenem and meropenem. Following a plausible route visited by the compounds during the binding process, the PP is probably touched before DP. Here, according to the docking results, meropenem penetrated more deeply in the protein than imipenem. The positions reached at the end of the MD simulations in the PP reflected even more different tendencies of the two carbapenems: imipenem had its β-lactam ring pointing toward the periplasmic region, meropenem pointed its ring toward the entrance to the DP. The different behavior of the two compounds can be explained in terms of their

dx.doi.org/10.1021/ja307803m | J. Am. Chem. Soc. 2012, 134, 19146−19158

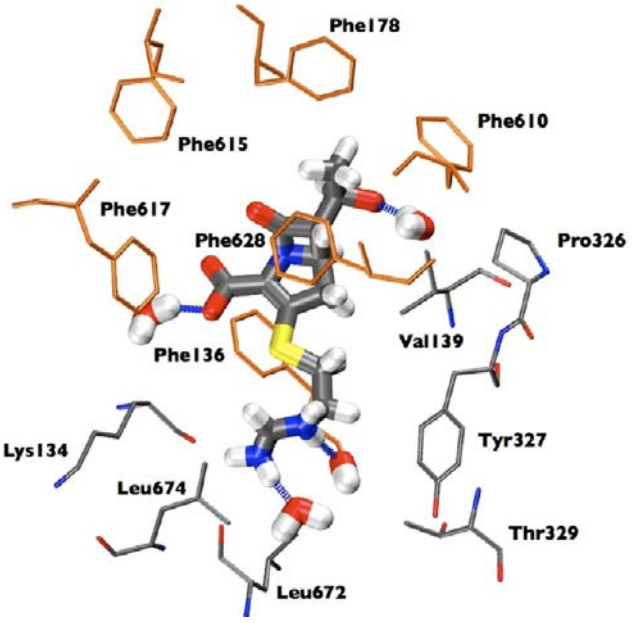

Figure 9. H-bond interactions between imipenem and slow waters. Imipenem and waters forming strong H-bond contacts are represented in thick licorice and colored by atom-code. H-bonds are evidenced by blue springs. The residues within 3 Å from the slow waters are colored by atom name. For clarity, the Phe residues of the DP are shown in orange-colored thin licorice.

propensity to interact with the solvent. During the simulations in the PP, imipenem explored the region around Thr859, which lies close to the outer leaflet of the cytoplasmic membrane and contains several water molecules in exchange with the periplasm (on average 8 within the first solvation shell of the residue). This region was not touched by meropenem, which essentially kept its position close to the border with the DP, as demonstrated by the statistically prominent interaction with Lys134. The pronounced hydrophilic character of imipenem was confirmed by the analysis of the interactions with the solvent. Imipenem was able to form long-lifetime interactions with water molecules inside of MexB, whereas meropenem was not. A further, although indirect, proof of the enhanced ability of imipenem to interact with the solvent came from the analysis of the ligand−residue interactions. Imipenem established a wide network of H-bonds also with residues of MexB, and meropenem essentially formed hydrophobic contacts (see Figures 7 and 8). Additionally, we performed calculations of the hydrophobic and hydrophilic properties for the most populated conformations of the two compounds in solution, PP and DP on the Platinum webserver.[102] Imipenem had always a larger polar portion of its surface (95.2 ± 0.4% in water, 94.1 ± 0.7% in the PP, 94.1 ± 0.6% in the DP) than meropenem (76.4 ± 2.1% in water, 87.2 ± 2.1% in the PP, 76.8 ± 1.2% in the DP).

In the DP, the second affinity site, the two compounds docked in similar positions but their trajectories during the 50 ns-long simulations led them to configurations that preluded diverse fates. Imipenem slid toward the bottom of the DP going away from the *Channel* entrance into a position similar to that assumed by doxorubicin in mutated AcrB F610A.[51] Doxorubicin, usually extruded by wild type AcrB, is inefficiently transported by the F610A variant, leading to a drastically reduced minimum inhibitory concentration (MIC).[103] Computer simulations indicated that upon mutation of residue 610 in the DP doxorubicin moves deeper into the pocket and is not extruded by the induced functional rotation.[51] In contrast to imipenem, in the DP, meropenem moved toward the *Channel* entrance, assuming thus a location more suited for the extrusion.

Our values of the binding free energy of imipenem in the DP and in the PP were very similar and positive (0.6 and 0.4 kcal/mol, respectively), supporting the idea of a compound that has no pronounced affinity for a particular site of the transporter (in particular for DP). Meropenem interacted differently with MexB, as it clearly preferred the DP (binding free energy of −8.1 kcal/mol) over the PP (binding free energy of 2.4 kcal/mol).

Evaluation of the RMSF pointed out another interesting aspect regarding the behavior of the two compounds. As shown in Figure 6, meropenem exhibited essentially the same fluctuations in the PP as in a water box. These fluctuations were larger than those characterizing the same compound in the DP. Probably, the less hydrophilic character of meropenem increased the fluctuations of the molecule in regions with a remarkable density of water molecules. Compared to meropenem, the atoms of imipenem underwent in both the PP and the water box smaller fluctuations, whose amplitudes differed only slightly from those in DP. The trend indicated how the presence of water stabilized the fluctuations of imipenem, also in DP, where slow waters resided only close to imipenem but not to meropenem. Additionally, the similar behavior of imipenem in the two affinity sites, PP and DP, suggested a lack of a preference for one or the other.

The results we presented were obtained on the T monomer of MexB, proposed to be in a configuration responsible for tight binding of the substrate in the designated binding pocket. In this monomer the conformation of the hydrophobic DP is such that it can well accommodate ligands. In fact, our docking protocol found more poses in this monomer than in the DP of the other ones. Therefore, our findings are consistent with the assumption that this region is the tight substrate binding pocket inside the periplasmic domain. Our docking results support the idea of a DP in AcrB and MexB able to bind substrates belonging to different chemical families. Moreover, we showed that binding of low-molecular-mass compounds to the PP in the T monomer is not so likely to occur. This is consistent with the common idea of a three-stroke functional rotation mechanism, where low affinity binding of small-weight substrates should occur in the L configuration of the transporter. Our docking protocol was not able to capture relevant binding geometries of either imipenem nor meropenem in the L monomer. The lack of such docking poses was most likely a consequence of the peculiarities of the MexB crystal structure.[40] The structure of MexB exhibits an L monomer characterized by a very narrow PP, whose size does not allow the entrance of substrates. The analogous PP site in the crystal structures of AcrB is larger and able to accommodate compounds as demonstrated very recently.[38,41] It is quite surprising that AcrB and MexB differ so largely only in this monomer, due to the high degree of similarity and homology of the two transporters. Thus, it is not clear if the narrow structure in MexB's L monomer is an artifact of the crystallization procedure or an indication of a different involvement of the monomers in the extrusion process. Further studies on the structure of MexB may shed light on this very intriguing issue. Our calculations suggested a less favorable interactions for

meropenem than imipenem in the PP of the T configuration. Unlike meropenem, imipenem showed the same low affinities for both DP and PP. We mostly found imipenem in the topological region of the DP closer to the PP than to the *Channel*. Therefore, residence in the DP for a time sufficiently long to activate transduction into the channel toward OprM is less likely to occur for imipenem than for meropenem. Hence, meropenem is more readily transported by MexB than imipenem. This finding is in accordance with data showing a 4- to 8-fold increase in the MIC of meropenem upon overexpression of MexB in *P. aeruginosa*, whereas the MIC for imipenem remains essentially the same.[18,104−107]

■ CONCLUSIONS

We performed a thorough computational study of meropenem and imipenem, two antibiotics of the carbapenem family whose activities are known to be differently affected by MexB. By analyzing the interaction patterns of the two compounds with the protein, we were able to build a microscopically well-founded model for the interaction of both drugs with MexB. The model offers a reliable explanation for the different effects of MexB on the antibacterial activities of imipenem and meropenem and sheds light on the elusive link between affinity and transport properties.

Our results highlight a strong difference in the binding properties of the two compounds in the DP. In particular, meropenem shows high affinity to this protein site, and assumes conformations in the pocket that prelude to efficient transduction toward the extrusion channel. On the other hand, imipenem does not bind to DP with good affinity, and explores geometries that are similar to those reported in AcrB mutants for poor transducing substrates. The different behaviors of the two carbapenems are associated with the different chemical-physical properties of the tails of the two compounds. The bulky and more hydrophobic groups in meropenem ensure better interactions with the aromatic-hydrophobic environment of the DP, while the more flexible and more hydrophilic tail of imipenem does not provide good affinity to the DP. A role of major importance is played by the interaction with the solvent, which largely contributes to the different transport properties of the two carbapenems. In fact, the compounds remain highly solvated in all binding sites explored in our studies. Nonetheless, the water dynamics around meropenem is significantly different in the DP than in the bulk solvent. On the contrary, imipenem shows the same interactions with solvent in the DP and in the bulk.

Our study suggests that the PP is a poor substrate binding site for MexB monomers in the T conformation for either meropenem or imipenem. Interestingly, in AcrB the PP in the L conformation has been postulated as an affinity site for large-molecular-mass compounds.[38,41] The reported X-ray structure for MexB shows a PP in the L conformer different from that of the homologous protein in *E. coli*. In particular, the PP in the L conformation is closed, and does not allow accommodation of any substrate there. In our docking search, we do not find any poses of the two drugs in the PP of the L monomer. Whether this evidence must be attributed to artifacts in the X-ray structure of MexB due to crystallization conditions, or instead, it implies a different mechanism for drug recognition and binding between AcrB and MexB remains to be defined by further studies, and possibly, by the determination of new X-ray structures of MexB.

Drugs evading efflux and inhibitors able to hamper the function of efflux systems may be designed more efficiently if based on microscopic knowledge of the dynamical interactions between drugs and pumps such as that achieved in the present study.

■ ASSOCIATED CONTENT

Supporting Information

Table containing the residues of MexB within 3 Å from carbapenem and imipenem in the poses extracted from docking to the PP and the DP, docking poses located in the *Channel*, RMSD of MexB, time evolution of distances between the centers of mass of the compounds and the center of mass of DP and *Gate*, time evolution of the position of the centers of mass of the compounds in the DP. This material is available free of charge via the Internet at http://pubs.acs.org.

■ AUTHOR INFORMATION

Corresponding Author

paolo.ruggerone@dsf.unica.it; michele.cascella@iac.unibe.ch

Notes

The authors declare no competing financial interest.
JD is an employee of Basilea Pharmaceutica International Ltd.

■ ACKNOWLEDGMENTS

We thank H. Nikaido (Berkeley) M. Stenta (EPFL, Lausanne), and E. Spiga (EPFL, Lausanne) for useful discussions, M. Dessalvi (Cagliari) for technical support, and Cineca for CPU time (ISCRA grant). The research of F. Collu and M. Cascella was funded by the Swiss National Science Foundation (Grant N. PP02-118930). A.V. Vargiu acknowledges financial support from *Regione Autonoma della Sardegna* through a Research Fellow on fundings *PO Sardegna FSE 2007-2013, L.R.7/2007 Promozione della ricerca scientifica e dell'innovazione tecnologica in Sardegna*.

■ REFERENCES

(1) Rice, L. B. *Biochem. Pharmacol.* **2006**, *71*, 991−995.
(2) Falagas, M. E.; Bliziotis, I. A. *Int. J. Antimicrob. Agents* **2007**, *29*, 630−636.
(3) Chopra, I.; Schofield, C.; Everett, M.; O'Neill, A.; Miller, K.; Wilcox, M.; Frère, J.-M.; Dawson, M.; Czaplewski, L.; Urleb, U.; Courvalin, P. *Lancet Infect. Dis.* **2008**, *8*, 133−139.
(4) Blot, S.; Depuydt, P.; Vandewoude, K.; De Bacquer, D. *Curr. Opin. Infect. Dis.* **2007**, *20*, 391−396.
(5) Gandhi, T. N.; DePestel, D. D.; Collins, C. D.; Jerod Nagel, J. N.; Washer, L. L. *Crit. Care Med.* **2010**, *38*, S315−S323.
(6) Tiwari, V.; Nagpal, I.; Subbarao, N.; Moganty, R. R. *J. Mol. Model.* **2012**, *18*, 3351−3361.
(7) Flamm, R.; Weaver, M.; Thornsberry, C.; Jones, M.; Karlowsky, J.; Sahm, D. *Antimicrob. Agents Chemother.* **2004**, *48*, 2431−2436.
(8) Hirsch, E. B.; Tam, V. H. *Expert Rev. Pharmacoecon. Outcomes Res.* **2010**, *10*, 441−451.
(9) de Bentzmann, S.; Plésiat, P. *Environ. Microbiol.* **2011**, *13*, 1655−1665.
(10) Breidenstein, E. B. M.; de la Fuente-Núñez, C.; Hancock, R. E. W. *Trends Microbiol.* **2011**, *19*, 419−426.
(11) Harris, A.; Torres-Viera, C.; Venkataraman, L.; DeGirolami, P.; Samore, M.; Y, C. *Clin. Infect. Dis.* **1997**, *28*, 1128−1133.
(12) Hsueh, P.; Teng, L.; Yang, P.; Chen, U.; Ho, S.; Luh, K. *J. Clin. Microbiol.* **1998**, *36*, 1347−1351.
(13) Verweij, P.; Bijl, D.; Melchere, W.; De Pauw, B.; Meis, J.; Hoogkamp-Korstanje, J.; Voss, A. *Infect. Control Hosp. Epidemiol.* **1997**, *18*, 128−131.

(14) Richard, P.; LeFloch, R.; Chamoux, C.; Pannier, M.; Espaze, E.; H, R. *J. Infect. Dis.* **1994**, *170*, 377−383.
(15) Bert, F.; Maubec, E.; Bruneau, B.; Berry, P.; Lambert-Zechovsky, N. *Emerging Infect. Dis.* **1998**, *39*, 53−62.
(16) Tacconelli, E.; Tumbarello, M.; Bertagnolio, S.; Citton, R.; Spanu, T.; Fadda, G.; Cauda, R. *Emerging Infect. Dis.* **2002**, *8*, 220−221.
(17) Arruda, E.; Marinho, I.; Boulos, M.; Sinto, S.; Caiaffa, H.; Mendes, C.; Oplustil, C.; Sader, H.; Levy, C.; Levin, A. *Infect. Control Hosp. Epidemiol.* **1999**, *20*, 620−623.
(18) Livermore, D. M. *Clin. Infect. Dis.* **2002**, *34*, 634−640.
(19) Poole, K. *Front. Microbiol.* **2011**, *2*, 65.
(20) Li, X.-Z.; Nikaido, H. *Drugs* **2009**, *69*, 1555−1623.
(21) Nikaido, H. *Annu. Rev. Biochem.* **2009**, *78*, 119−146.
(22) Piddock, L. J. V. *Clin. Microbiol. Rev.* **2006**, *19*, 382−402.
(23) Poole, K. *Ann. Med.* **2007**, *39*, 162−176.
(24) Davin-Regli, A.; Bolla, J.-M.; James, C. E.; Lavigne, J.-P.; Chevalier, J.; Garnotel, E.; Molitor, A.; Pagès, J.-M. *Curr. Drug Targets* **2008**, *9*, 750−759.
(25) Ceccarelli, M.; Ruggerone, P. *Curr. Drug Targets* **2008**, *9*, 779−788.
(26) Pagès, J.-M.; James, C. E.; Winterhalter, M. *Nat. Rev. Microbiol.* **2008**, *6*, 893−903.
(27) Pagès, J.; Amaral, L. *Biochim. Biophys. Acta* **2009**, *1794*, 826−833.
(28) Nikaido, H.; Pagès, J.-M. *FEMS Microbiol. Rev.* **2011**, *36*, 340−363.
(29) Okamoto, K.; Gotoh, N.; Nishino, T. *J. Infect. Chemother.* **2002**, *8*, 371−373.
(30) Blair, J. M. A.; Piddock, L. J. V. *Curr. Opin. Microbiol.* **2009**, *12*, 512−519.
(31) Lomovskaya, O.; Zgurskaya, H. I.; Totrov, M.; Watkins, W. J. *Nat. Rev. Drug Discovery* **2007**, *6*, 56−65.
(32) Xu, Y.; Moeller, A.; Jun, S.-Y.; Le, M.; Yoon, B.-Y.; Kim, J.-S.; Lee, K.; Ha, N.-C. *J. Biol. Chem.* **2012**, *287*, 11740−11750.
(33) Murakami, S.; Nakashima, R.; Yamashita, E.; Yamaguchi, A. *Nature* **2002**, *419*, 587−593.
(34) Murakami, S.; Nakashima, R.; Yamashita, E.; Matsumoto, T.; Yamaguchi, A. *Nature* **2006**, *443*, 173−179.
(35) Seeger, M. A.; Schiefner, A.; Eicher, T.; Verrey, F.; Diederichs, K.; Pos, K. M. *Science* **2006**, *313*, 1295−1298.
(36) Sennhauser, G.; Amstutz, P.; Briand, C.; Storchenegger, O.; Grütter, M. G. *PLoS Biol.* **2007**, *5*, e7.
(37) Seeger, M. A.; Von Ballmoos, C.; Eicher, T.; Brandstätter, L.; Verrey, F.; Diederichs, K.; Pos, K. M. *Nat. Struct. Mol. Biol.* **2008**, *15*, 199−205.
(38) Nakashima, R.; Sakurai, K.; Yamasaki, S.; Nishino, K.; Yamaguchi, A. *Nature* **2011**, *480*, 565−569.
(39) Murakami et al.[34] and Sennhauser et al.[36] adopted a different notation: For Sennhauser et al., A corresponds to L, B to T, and C to O, for Murakami et al., A corresponds to T, B to O, and C to L.
(40) Sennhauser, G.; Bukowska, M. A.; Briand, C.; Grütter, M. G. *J. Mol. Biol.* **2009**, *389*, 134−145.
(41) Eicher, T.; Cha, H.-J.; Seeger, M. A.; Brandstätter, L.; El-Delik, J.; Bohnert, J. A.; Kern, W. V.; Verrey, F.; Grütter, M. G.; Diederichs, K.; Pos, K. M. *Proc. Natl. Acad. Sci. U.S.A.* **2012**, *109*, 5687−5692.
(42) Simmons, K. J.; Chopra, I.; Fishwick, C. W. G. *Nat. Rev. Microbiol.* **2010**, *8*, 501−510.
(43) Wereszczynski, J.; McCammon, J. A. *Q. Rev. Biophys.* **2012**, *45*, 1−25.
(44) McGeagh, J. D.; Ranaghan, K. E.; Mulholland, A. J. *Biochim. Biophys. Acta* **2011**, *1814*, 1077−1092.
(45) Biarnés, X.; Bongarzone, S.; Vargiu, A. V.; Carloni, P.; Ruggerone, P. *J. Comput.-Aided Mol. Des.* **2011**, *25*, 395−402.
(46) Leone, V.; Marinelli, F.; Carloni, P.; Parrinello, M. *Curr. Opin. Struc. Biol.* **2010**, *20*, 148−154.
(47) Christ, C. D.; Mark, A. E.; van Gunsteren, W. F. *J. Comput. Chem.* **2010**, *31*, 1569−1582.
(48) Schulz, R.; Vargiu, A. V.; Collu, F.; Kleinekathoefer, U.; Ruggerone, P. *PLoS Comput. Biol.* **2010**, *6*, e1000806.
(49) Yao, X.-Q.; Kenzaki, H.; Murakami, S.; Takada, S. *Nat. Commun.* **2010**, *1*, 117.
(50) Schulz, R.; Vargiu, A. V.; Ruggerone, P.; Kleinekathöfer, U. *J. Phys. Chem. B* **2011**, *115*, 8278−8287.
(51) Vargiu, A. V.; Collu, F.; Schulz, R.; Pos, K. M.; Zacharias, M.; Kleinekathöfer, U.; Ruggerone, P. *J. Am. Chem. Soc.* **2011**, *133*, 10704−10707.
(52) Fischer, N.; Kandt, C. *Proteins* **2011**, *79*, 2871−2885.
(53) Page, M. G. P.; Heim, J. *Curr. Opin. Pharmacol.* **2009**, *9*, 558−565.
(54) Papp-Wallace, K. M.; Endimiani, A.; Taracila, M. A.; Bonomo, R. A. *Antimicrob. Agents Chemother.* **2011**, *55*, 4943−4960.
(55) Zhanel, G.; Wiebe, R.; Dilay, L.; Thomson, K.; Rubinstein, E.; Hoban, D.; Noreddin, A.; Karlowsky, J. *Drugs* **2007**, *67*, 1027−1052.
(56) Spellberg, B.; Guidos, R.; Gilbert, D.; Bradley, J.; Boucher, H. W.; Scheld, W. M.; Bartlett, J. G.; Edwards, J.; Infection Diseases Society of America. *Clin. Infect. Dis.* **2008**, *46*, 155−164.
(57) Gootz, T. D. *Crit. Rev. Immunol.* **2010**, *30*, 79−93.
(58) Silver, L. L. *Clin. Microbiol. Rev.* **2011**, *24*, 71−109.
(59) Masuda, N.; Ohya, S. *Antimicrob. Agents Chemother.* **1992**, *36*, 1847−1851.
(60) Pai, H.; Kim, J.; Kim, J.; Lee, J. H.; Choe, K. W.; Gotoh, N. *Antimicrob. Agents Chemother.* **2001**, *45*, 480−484.
(61) Pournaras, S.; Maniati, M.; Spanakis, N.; Ikonomidis, A.; Tassios, P. T.; Tsakris, A.; Legakis, N. J.; Maniatis, A. N. *J. Antimicrob. Chemother.* **2005**, *56*, 761−764.
(62) Walsh, F.; Amyes, S. G. B. *J. Chemother.* **2007**, *19*, 376−381.
(63) Nagano, K.; Nikaido, H. *Proc. Natl. Acad. Sci. U.S.A.* **2009**, *106*, 5854−5858.
(64) Lim, S. P.; Nikaido, H. *Antimicrob. Agents Chemother.* **2010**, *54*, 1800−1806.
(65) Ceccarelli, M.; Vargiu, A. V.; Ruggerone, P. *J. Phys.: Condens. Matter* **2012**, *24*, 104012.
(66) Sali, A.; Blundell, T. L. *J. Mol. Biol.* **1993**, *234*, 779−815.
(67) Eswar, N.; Webb, B.; Marti-Renom, M. A.; Madhusudhan, M. S.; Eramian, D.; Shen, M.-Y.; Pieper, U.; Sali, A. *Curr. Protoc. Protein Sci.* **2007**, *Chapter 2*, No. Unit 2.9.
(68) Cornell, W. D.; Cieplak, P.; Bayly, C. I.; Gould, I. R., Jr.; K., M. M.; DM, D. M. F.; Spellmeyer, D. C.; Fox, T.; Caldwell, J. W.; Kollman, P. A. *J. Am. Chem. Soc.* **1995**, *117*, 5179−5197.
(69) Cheatham, T.; Cieplak, P.; Kollman, P. *J. Biomol. Struct. Dyn.* **1999**, *16*, 845−862.
(70) Jorgensen, W. L.; Chandrasekhar, J.; Madura, J. D.; Klein, M. L. *J. Chem. Phys.* **1983**, *79*, 926−935.
(71) Aaqvist, J. *J. Phys. Chem.* **1990**, *94*, 8021−8024.
(72) Phillips, J. C.; Braun, R.; Wang, W.; Gumbart, J.; Tajkhorshid, E.; Villa, E.; Chipot, C.; Skeel, R. D.; Kalé, L.; Schulten, K. *J. Comput. Chem.* **2005**, *26*, 1781−1802.
(73) Wang, J.; Wolf, R. M.; Caldwell, J. W.; Kollman, P. A.; Case, D. A. *J. Comput. Chem.* **2004**, *25*, 1157−1174.
(74) Fox, T.; A. Kollman, P. *J. Phys. Chem. B* **1998**, *102*, 8070−8079.
(75) Zacharias, M. *Proteins* **2005**, *60*, 252−256.
(76) May, A.; Zacharias, M. *Proteins* **2008**, *70*, 794−809.
(77) Hinsen, K. *Proteins* **1998**, *33*, 417−429.
(78) Humphrey, W.; Dalke, A.; Schulten, K. *J. Mol. Graphics* **1996**, *14*, 33−38.
(79) Essmann, U.; Perera, L.; Berkowitz, M. L.; Darden, T.; Lee, H.; Pedersen, L. G. *J. Chem. Phys.* **1995**, *103*, 8577−8593.
(80) Ryckaert, J. P.; Ciccotti, G.; Berendsen, H. J. C. *J. Comput. Phys.* **1977**, *23*, 327−341.
(81) Case, D. A.; Cheatham, T. E.; Darden, T.; Gohlke, H.; Luo, R.; Merz, K. M.; Onufriev, A.; Simmerling, C.; Wang, B.; Woods, R. J. *J. Comput. Chem.* **2005**, *26*, 1668−1688.
(82) Sterpone, F.; Ceccarelli, M.; Marchi, M. *J. Mol. Biol.* **2001**, *311*, 409−419.
(83) Venken, T.; Krnavek, D.; Muench, J.; Kirchhoff, F.; Henklein, F.; De Maeyer, M.; Voet, A. *Proteins* **2011**, *79*, 3221−3235.

(84) Kollman, P. A.; Massova, I.; Reyes, C.; Kuhn, B.; Huo, S.; Chong, L.; Lee, M.; Lee, T.; Duan, Y.; Wang, W.; Donini, O.; Cieplak, P.; Srinivasan, J.; Case, D. A.; Cheatham, T. E., III. *Acc. Chem. Res.* **2000**, *33*, 889−897.
(85) Kuhn, B.; Kollman, P. A. *J. Med. Chem.* **2000**, *43*, 3786−3791.
(86) Kuhn, B.; Gerber, P.; Schulz-Gasch, T.; Stahl, M. *J. Med. Chem.* **2005**, *48*, 4040−4048.
(87) Hou, T.; Wang, J.; Li, Y.; Wang, W. *J. Chem. Inf. Model.* **2011**, *51*, 69−82.
(88) Karplus, M.; Kushick, J. N. *Macromolecules* **1981**, *14*, 325−332.
(89) Baron, R.; van Gunsteren, W. F.; Hünenberger, P. H. *Trends Phys. Chem.* **2006**, *11*, 87−122.
(90) Baron, R.; Hünenberger, P. H.; McCammon, J. A. *J. Chem. Theory Comput.* **2009**, *5*, 3150−3160.
(91) Chang, C.-E.; Chen, C.; Gilson, M. K. *J. Chem. Theory Comput.* **2005**, *1*, 1017−1028.
(92) Andricioaei, I.; Karplus, M. *J. Chem. Phys.* **2001**, *115*, 6289−6292.
(93) Carlsson, J.; Aqvist, J. *J. Phys. Chem. B* **2005**, *109*, 6448−6456.
(94) Yu, E. W.; McDermott, G.; Zgurskaya, H. I.; Nikaido, H.; Koshland, D. E. *Science* **2003**, *300*, 976−980.
(95) Murakami, S.; Tamura, N.; Saito, A.; Hirata, T.; Yamaguchi, A. *J. Biol. Chem.* **2004**, *279*, 3743−3748.
(96) Yu, E. W.; Aires, J. R.; McDermott, G.; Nikaido, H. *J. Bacteriol.* **2005**, *187*, 6804−6815.
(97) Su, C.-C.; Li, M.; Gu, R.; Takatsuka, Y.; McDermott, G.; Nikaido, H.; Yu, E. W. *J. Bacteriol.* **2006**, *188*, 7290−7296.
(98) Das, D.; Xu, Q. S.; Lee, J. Y.; Ankoudinova, I.; Huang, C.; Lou, Y.; DeGiovanni, A.; Kim, R.; Kim, S.-H. *J. Struct. Biol.* **2007**, *158*, 494−502.
(99) Seeger, M. A.; Diederichs, K.; Eicher, T.; Brandstätter, L.; Schiefner, A.; Verrey, F.; Pos, K. M. *Curr. Drug Targets* **2008**, *9*, 729−749.
(100) Pos, K. M. *Biochim. Biophys. Acta* **2009**, *1794*, 782−793.
(101) Husain, F.; Bikhchandani, M.; Nikaido, H. *J. Bacteriol.* **2011**, *193*, 5847−5849.
(102) Pyrkov, T. V.; Chugunov, A. O.; Krylov, N. A.; Nolde, D. E.; Efremov, R. G. *Bioinformatics* **2009**, *25*, 1201−1202.
(103) Bohnert, J. A.; Schuster, S.; Seeger, M. A.; Fähnrich, E.; Pos, K. M.; Kern, W. V. *J. Bacteriol.* **2008**, *190*, 8225−8229.
(104) Eguchi, K.; Ueda, Y.; Kanazawa, K.; Sunagawa, M.; Gotoh, N. *J. Antibiot.* **2007**, *60*, 129−135.
(105) Ong, C. T.; Tessier, P. R.; Li, C.; Nightingale, C. H.; Nicolau, D. P. *Diagn. Microbiol. Infect. Dis.* **2007**, *57*, 153−161.
(106) Mesaros, N.; Glupczynski, Y.; Avrain, L.; Caceres, N. E.; Tulkens, P. M.; Van Bambeke, F. *J. Antimicrob. Chemother.* **2007**, *59*, 378−386.
(107) Riera, E.; Cabot, G.; Mulet, X.; García-Castillo, M.; Del Campo, R.; Juan, C.; Cantón, R.; Oliver, A. *J. Antimicrob. Chemother.* **2011**, *66*, 2022−2027.